Study of the formation of 3-D titania nanofibrous structure by MHz femtosecond laser in ambient air

Amirhossein Tavangar, Bo Tan, and K. Venkatakrishnan

Articles you may be interested in

Surface area and porosity in obliquely grown photocatalytic titanium dioxide for air purification
J. Appl. Phys. **115**, 174907 (2014); 10.1063/1.4874918

Structurally stabilized mesoporous TiO2 nanofibres for efficient dye-sensitized solar cells
APL Mat. **1**, 032106 (2013); 10.1063/1.4820425

Multi-band photoluminescence in TiO2 nanoparticles-assembled films produced by femtosecond pulsed laser deposition
J. Appl. Phys. **114**, 043503 (2013); 10.1063/1.4816251

Nanostructures synthesis by femtosecond laser ablation of glasses
J. Appl. Phys. **112**, 073109 (2012); 10.1063/1.4754864

Photocatalytic properties of porous titania grown by oblique angle deposition
J. Appl. Phys. **111**, 074904 (2012); 10.1063/1.3699370

Study of the formation of 3-D titania nanofibrous structure by MHz femtosecond laser in ambient air

Amirhossein Tavangar,[1] Bo Tan,[2] and K. Venkatakrishnan[1]

[1]*Department of Mechanical and Industrial Engineering, Ryerson University, Toronto, ON M5B 2K3, Canada*
[2]*Department of Aerospace Engineering, Ryerson University, Toronto, ON M5B 2K3, Canada*

In this study, we describe the formation mechanism of web-like three-dimensional (3-D) titania nanofibrous structures during femtosecond laser ablation of titanium (Ti) targets in the presence of background air. First, we demonstrate the mechanism of ablation of Ti targets by multiple femtosecond laser pulses at ambient air in an explicit analytical form. The formulas for evaporation rates and the number of ablated particles, which is analogous to the deposition rate of the synthesized nanofibers, for the ablation by a single pulse and multiple pulses as a function of laser parameters, background gas, and material properties are predicted and compared to experimental results. Afterwards, the formation of nanofibrous structures is demonstrated by applying an existing simplified kinetic model to Ti targets and ambient conditions. The predicted theory provides nanofiber diameter dependency with the combination of laser parameters, target properties, and ambient gas characteristics. Experimental studies are then performed on titania nanofibrous structures synthesized by laser ablation of Ti targets using MHz repletion-rate femtosecond laser at ambient air. The models' predictions are then compared with the experimental results, where nanostructures with different morphologies are manufactured by altering laser parameters. Our results indicate that femtosecond laser ablation of Ti targets at air background yields crystalline titania nanostructures. The formation of crystalline titania nanostructures is preceded by thermal mechanism of nucleation and growth. The results point out that laser pulse repetition and dwell time can control the density, size, and pore size of the engineered nanofibrous structure. As the deposition rate of nanostructures is analogous to the ablation rate of the target, higher density of nanofibrous structure is seen at greater laser fluences. The predicted theory can be applied to predict ablation mechanism and nanofiber formation of different materials. © *2013 American Institute of Physics*. [http://dx.doi.org/10.1063/1.4771667]

I. INTRODUCTION

Nanostructures have recently drawn great attention due to the exceptional physical, optical, and chemical properties they present, compared to those of their bulk counterparts. Nanostructures, in different forms, can be utilized for the development of different technological applications. In particular, titanium dioxide (titania) nanostructures have attracted lots of interest owing to their outstanding mechanical and thermal properties, biocompatibility, and corrosion resistance.[1,2] They have been widely exploited in numerous technologies including implantable drug delivery systems,[3,4] biosensors,[5,6] solar cells,[7,8] photocatalysis,[9,10] tissue engineering,[11,12] and other medical devices.[6,13]

Various preparation techniques have been developed for the synthesis of titania nanostructures such as anodization,[14] chemical vapour synthesis,[15] hydrothermal methods,[16] so-gel,[17] and template-based synthesis.[18] Negative[19,20] and positive[21,22] templating approaches have been implemented to generate titania nanotubes with uniform length and diameter. It has been reported that the dimension of nanotubes could be controlled by the type and dimension of the utilized templates. Nonetheless, both of these template-assisted techniques are incompetent to achieve small nanotubes easily due to the restriction of the pore size of the mold prepared from porous materials such as

alumina.[23,24] In addition, the templating approaches often suffer from long cumbrous prefabrication and template post-removal processes. Also, since the removal of the templates is performed using chemical mediums, it may result in nanostructure contamination as impurities cannot be completely eliminated during the process.[21,25] Anodization method also has been commonly used to fabricate high aspect ratio titania nanotubes.[25] Several studies have reported that the dimension of nanotubes can be controlled by altering the applied voltage, pH and anodizing time, and electrolyte composition.[26,27] However, the as-synthesized nanotubes are amorphous, and a post-annealing treatment is required to crystallize them into titania nanostructures.[28] Furthermore, some studies have pointed out that the post-annealing treatment has adverse effects on the stability of the nanostructures.[29] High temperatures during post-annealing process may lead to the disposition and the solid-state sintering of high aspect ratio nanotubes, resulting in grain growth, densification, and consequently complete collapse of the structures.[30] Hydrothermal methods have been of interest, as they produce pure crystalline titania nanostructures.[28] The starting materials, pre-treatment process, hydrothermal temperature, and post-treatment process can influence the formation of titania nanostructures using hydrothermal methods.[31,32] Nevertheless, this nanofabrication method has been reported to require long reaction times and NaOH post-treatment, which may result in

excessive intercalation leading to the generation of delicate non-aligned nanotubes.[25,28] In addition to aforementioned drawbacks, these traditional routes also are limited to the fabrication of 1-D and 2-D nanostructures and suffer from expensive precursors, long processing time, and uncontrollable phase transformation during chemical routes.[33,34] These drawbacks seem to be harmful to titania nanostructure practical applications.

Laser ablation has proven to be an effective technique for synthesizing nanostructures of various shape and internal structure on different materials.[35,36] Extensive studies have been reported on synthesis of different titania nanostructures, including nanoparticle, nanotube, nanofibers, nanorod, and nanowirez, using laser processing.[17,33,37,38] However, special conditions are often required to promote a particular type of structure to grow. For instance, the synthesis of nanotubes by a low-repetition-rate nanosecond laser needs to be performed in a furnace with high controlled temperature and under continuous noble gas stream as the laser plume cools down after the pulse below the minimal temperature required for the nanotube formation. On the other hand, the introduction of megahertz (MHz) repetition-rate ultrashort lasers allows eliminating additional heating and the need for the ambient gas in the chamber.[39] MHz Femtosecond lasers, along with a better understanding of the physics of ultrashort laser-matter interaction, facilitate the synthesis of nanostructures which previously could not be produced by traditional long laser pulses. Femtosecond laser pulses heat materials to higher pressure and temperature than do longer-pulse lasers of comparable fluences as the energy is delivered before significant thermal conduction happens in the materials.[40,41] Therefore, a femtosecond laser pulse can heat any material to a solid-density plasma state with temperature and pressure above the critical point. This leads to the generation of high density plume which results in nanoparticle aggregation after plume condensation.

In previous study, we have introduced a single-step method to synthesize 3-D titania nanofibrous structures under high repetition femtosecond laser irradiation at ambient conditions.[38] We have reported that this method would enable us to synthesize 3-D interwoven nanoarchitectures that incorporate the functions of 3-D nano-scaled topography and modified physiochemical properties to promote Ti interfacial characteristics for developing new functional biomaterials. Our previous results indicated that the morphology of the nanostructures could be controlled by altering laser parameters. As it follows, this study demonstrates the ablation mechanism of Ti targets by multiple femtosecond laser pulses at ambient air in an explicit analytical form. The formulas for evaporation rates and the number of ablated particles for laser ablation by a single pulse as well as multiple pulses as a function of laser parameters, background gas, and material properties are predicted and compared to experimental results. Later, the formation mechanism of the nanofibrous structures during femtosecond laser ablation of Ti targets in the presence of air is discussed. This study also describes the formation of nanofibrous structures by applying an existing simplified kinetic model to Ti targets and ambient conditions. The customized theory predicts the depend-ency of the fabricated nanofiber on the laser and background gas properties. Finally, experimental studies are conducted on titania nanofibrous structures synthesized by laser ablation of Ti targets using MHz repletion-rate femtosecond laser at ambient air. Then, the predictions of the models are compared with the experimental results where nanostructures with different morphologies are synthesized by altering laser parameters.

II. ABLATION MECHANISM BY A SINGLE ULTRASHORT LASER PULSE IN AMBIENT GAS

It has been reported that material ablation in air takes place at lower ablation thresholds compared with it in the vacuum.[42] It was reported that in the presence of air background, collisions between the ambient gas atoms and the surface decreases the lifetime of the non-equilibrium regime which establishes thermal evaporation. Once the laser pulse interacted with the target, the air next to its heated surface collides with the target surface and obtains energy required for the formation of a Maxwell distribution in the air in close vicinity of the target surface. In other words, the presence of air leads to the establishment of a high-energy tail Maxwell distribution in the surface layer increasing the bulk-to-surface energy transfer. It was assumed that only the air-surface collision plays a role for thermal evaporation from the surface as the bulk-to surface energy transfer time is much longer than the air-solid equilibrium time.

The air-solid equilibrium energy distribution is started by air molecules-solid collision. Considering the gas-kinetic mean free path in air in standard conditions ($l_{g-k} = 6 \times 10^{-6}$ cm),[43] the equilibration time t_{eq} required to form a Maxwell distribution in air can be estimated to be $t_{eq} \sim 1.8 \times 10^{-10}$, using $t_{eq} \approx t_{g-k} \approx l_{g-k}/v_{th}$. The average thermal velocity v_{th} in air is approximately $v_{th} = 3.3 \times 10^4$ cm/s at room temperature.[42] According to previous studies, the bulk-to-surface energy transfer time at the maximum temperature for the threshold fluence conditions in air is calculated to be $t_{b-s} \sim 30$ ns $\gg t_{eq}$ for several metal targets (i.e., Cu, Al, and Fe) after the end of the laser pulse.[44] Therefore, as the bulk-to-surface energy transfer time is much longer than the air-solid equilibrium time, it is assumed that only the air-surface collisions play a role for thermal evaporation from the surface.

Thermal evaporation would initiate sometime after the equilibration time $t > t_{eq}$. At this equilibration time, the solid-air interface temperature equilibration is completed and continues to fall according to the linear heat conduction law. Assuming the vapor-air mixture with a predominance of air plays the role of the saturated vapor over the ablated solid, the thermal evaporation can be estimated as:[44]

$$\langle R_{evp}\rangle_{therm} \approx n_{air}\left(\frac{k_B T_{max}}{2\pi M_a}\right)^{1/2} (t_p t_{eq})^{1/2}\left[\frac{\text{atoms}}{\text{cm}^2}\right], \quad (1)$$

where T_{max} is the maximum temperature at the end of the laser pulse that could be calculated at the experimentally determined threshold fluence in air. A simple way to estimate the maximum temperature, however, is to consider that the target is heated by a single laser pulse in a heat conduction regime where all losses due to radiation and plume

expansion can be neglected. Hence, the heating process can be modeled as propagation of a heat wave into the target according to the one-dimensional (1-D) heat conduction regime:[41,45]

$$\langle T \rangle = \left(\frac{2}{\pi}\right)^{1/2} \frac{I_a(at_p)^{1/2}}{k_h} = \frac{1}{2^{1/2}} T(0, t_p). \quad (2)$$

One should note that the maximum target temperature occurs at the end of the laser pulse, i.e., $T_{max} = T(0, t_p)$. Thus, T_{max} can be written as

$$T_{max} = \frac{2I_a(at_p)^{1/2}}{k_h(\pi)^{1/2}}. \quad (3)$$

The absorbed laser intensity on the target surface $I_a = AI_0$ can be obtained by having the intensity of incident pulse and laser absorption coefficient.

The intensity of the incident laser pulse (I_0) may be calculated by measuring the laser average power P_{ave} as follows:

$$I_0 = \frac{P_{avg}}{R_{rep}t_pA_{foc}}, \quad (4)$$

here, P_{avg} is average power (in W), measured directly from the incident laser pulse, R_{rep} (in s^{-1}) is laser repetition rate, and A_{foc} (in cm^2) is the irradiation focal spot area, which can be obtained by calculating the theoretical minimum laser spot diameter (D_0):[45,46]

$$D_0 \approx \frac{1.27\lambda_0 f}{D}, \quad (5)$$

where λ_0 is the wavelength of the laser, f is the effective focal length of the lens, and D denotes the laser beam diameter.

Using Eqs. (4) and (5), one can estimate the maximum temperature as a function of laser parameters:

$$T_{max} = \frac{2AP_{avg}a^{1/2}}{k_h R_{rep} A_{foc}(\pi t_p)^{1/2}}. \quad (6)$$

Then, the evaporation rate for single pulse ablation can be expressed by substituting Eq. (6) into Eq. (1) as follows:

$$\langle R_{evp} \rangle_{therm} \approx n_{air} \left(\frac{k_B a A t_{eq}^{3/2}}{M_a k_h \pi^{3/2}} \frac{P_{avg}}{R_{rep} A_{foc}}\right)^{1/2} \left[\frac{atoms}{cm^2}\right]. \quad (7)$$

The first part in the bracket depends on the target material properties, whereas the second part shows the evaporation rate dependency on the parameters of laser process.

III. ABLATION RATE IN CASE OF MULTIPLE LASER PULSES

One single ultrashort high intensity pulse would evaporate relatively a limited number of atoms per pulse.[47] However, for practical and industrial applications, laser systems with high average ablation rate are required.[48] For this rea-

son, laser systems with ultrahigh pulse (MHz) repetition rates are utilized to attain a high average ablation rate. Using MHz repetition rates, the focused laser beam dwells at a particular spot on the target for times longer than the time gap between the pulses. Therefore, multiple laser pulses arriving at the same spot on the target surface depends on the laser pulse dwell time (D_t), which leads to incubation of heating and evaporation process.

Now to define the number of evaporated atoms for multiple laser pulses, one should consider the number of pulses arriving at the same spot on the target in a specific dwell time. The number of atoms evaporated per single pulse can be expressed as follows:

$$N_P = R_{evp}A_{foc}[\text{atoms}]. \quad (8)$$

Then, the number of atoms evaporated from the same spot after successive pulses at the laser beam dwell time of D_t reads:

$$N_{MP} = N_P R_{rep} D_t = R_{evp} A_{foc} R_{rep} D_t \ [\text{atoms}]. \quad (9)$$

By substituting Eq. (7) into Eq. (9), the number of evaporated atoms by successive pulses based on the laser parameters and the target material properties can be estimated in the following form:

$$N_{MP} \approx n_{air} \left(\frac{k_B a A t_{eq}^{3/2}}{M_a k_h \pi^{3/2}}\right)^{1/2} (P_{avg} R_{rep} A_{foc})^{1/2} D_t[\text{atoms}] \quad (10)$$

One should note from Eq. (10) that the number of evaporated particles is a function of laser processing parameters, material properties, and ambient gas vapor density. The main factor is laser beam dwell time which linearly affects the evaporated atoms. The laser repetition rate influences the number of evaporated atoms by a square root.

As the laser beam dwell time is usually higher than the time between the two successive laser pulses in MHz-repletion regimes, multiple pulses arrive at the same spot. Consequently, the atomic flow into the plume would remain at levels required to generate nanostructures.

IV. NANOSTRUCTURE GROWTH IN AMBIENT AIR

The expanding plume of ablated material cools down adiabatically due to diffusion in the ambient air. Vapour condensation starts with nucleation, proceeds with growth of a supercritical nucleus, and comes to a halt by quenching. The density and temperature of evaporated atoms in the expanding plume are the main factors for formation of nanostructures. The diffusion and collision of evaporated atoms/ions with ambient gas atoms/ions at the high temperature early in the cooling process result in coalescence.[36] As the plume cools down, coalescence terminates and colliding particles are likely to form aggregates. The formation of nanostructures would go on through an aggregate-aggregate and atom-aggregate attachment over the period of time after the end of the laser pulse. The longer the plume of high density and temperature lasts, the more consecutive inelastic

collisions occur, which result in the formation of larger nanostructures. The plume diffusion time to the background air depends on the combination of laser parameters, material properties, and ambient condition. Previous studies, however, have pointed out that the diffusion time of the ablated material through the gas plays a major role in determining the cluster formation time and, thus, the nanostructure size.[49] Depending on the density of the evaporated atoms, different types of nanostructures, from individual particles to 3-D nanofibrous structures, can be formed and deposited on the substrate. Therefore, in order to synthesize 3-D nanofibrous structures, the continuous arrival of the laser pulses is necessary to keep the plume density at the critical level required for the formation of 3-D nanostructures. Previous studies have confirmed that only MHz laser pulse repetition rates lead to the formation of 3-D nanostructures.[38,39]

A simplified kinetic model of nanocluster formation may be applied to estimate the number of atoms in a nanostructure as a function of average plume parameters, based on the conservation of energy, momentum, and number of atoms in the generated plume after the end of the pulse. Accordingly, the size of the nanoparticles and the radius of the nanofibers could be predicted.[49] This model assumes that a nanocluster is formed through the neutral-neutral monomer inelastic sticky collisions and ignores the ion-ion, ion-neutral, and the other complex dusty-plasma collision effects. The first important step toward synthesis of a large nanostructure is the formation of dimers. The use of an ambient air with atmospheric pressure has the advantage of plume confinement, which increases the density of the component atoms in formation region leading to higher probability of sticky attachment. It has been stated that the diffusion plays the major role when the pressure of background gas approaches 10% of atmosphere pressure. Therefore, one can assume that in ambient air only diffusion-dominated expansion of the plume exists.

Diffusion of single titanium atoms in air of density n_{air} proceeds with diffusion velocity, $D_{dv} = l v_{Ti}/3 \approx v_{Ti}/(3 n_{air} \sigma_{Ti-air})$, where σ_{Ti-air} is the cross section for titanium-air elastic collision. Note that $Ti - air$ collision cross section is almost five times larger than that for $Ti - Ti$ collisions. The diffusion coefficient in the mixture of two gases depends on the total cross section σ_{total}, which is expressed as the following:

$$\sigma_{total} = \frac{\pi(d_1^2 + d_2^2)}{4}, \tag{11}$$

where d_1 and d_2 are diameters of particles in the mixture. In case of $Ti - Ti$ collision, the total cross section $\sigma_{Ti-Ti} = 0.31 \times 10^{-15}$ cm^2 (the atomic radius 140 pm; $d_{Ti} = 280$ pm). The cross section of titanium atoms and air (considering the radius of an oxygen atom, $d_{air} = 308$ pm) is $\sigma_{Ti-air} = 1.36 \times 10^{-15}$ cm^2. Thus, the formation of nanostructures mostly depends on the diffusion of Ti atoms in ambient air.

Following the model presented in Ref. 49, one may assume that the time for the formation of a nanofiber composed of N atoms equals to diffusion time, then the radius of a synthesized nanofiber reads:

$$r_{nanofiber} \approx B n_{Ti}^{-2/15} l_{abl}^{1/6} n_{air}^{3/10} (\sigma_{Ti-Ti} \sigma_{Ti-air})^{1/4} \left(\frac{T_{min}}{T_0}\right)^{1/20}, \tag{12}$$

here, $l_{abl} \equiv N_p/n_{Ti}A_{foc}$ is the ablation depth, B is a dimensionless numerical coefficient that should be estimated from the experiments, T_{min} is the minimum temperature for the nanostructure formation which is equal to the temperature in the mixture of Ti-air atoms after equilibrium, and $T_0 = T_{max}$ is the initial plume temperature. Therefore, the nanofiber radius depends on the air density, the cross section of target and ambient gas atoms, and the number of ablated atom estimated from Eq. (10), in the diffusion dominated conditions as follows:

$$r_{nanofiber} \approx B n_{Ti}^{-9/30} n_{air}^{3/10} (\sigma_{Ti-Ti} \sigma_{Ti-air})^{1/4}$$
$$\times \left(\frac{N_p}{A_{foc}}\right)^{1/6} \left(\frac{T_{min}}{T_0}\right)^{1/20}. \tag{13}$$

As one can see from Eq. (13), the main factor playing role in nanofiber size is the density of the ambient air, which affects the size approximately as a cubic root of the gas pressure.

V. EXPERIMENTAL DETAILS

The nanofibrous structures were synthesized on Ti specimens using single point femtosecond laser irradiation under ambient condition. Experiments were performed by a 1040 nm wavelength direct-diode-pumped Yb-doped fiber amplified MHz femtosecond laser system. The maximum output power of the laser was 15 W, the laser pulse width was 214 fs, and pulse repetition ranged from 200 kHz to 26 MHz. Because of solid state operation and high spatial mode quality of fiber lasers, the system operated under low noise performance. The laser parameters such as laser repetition rate, pulse width, and beam power were computer monitored which allowed a simple interaction with the performed experiments. However, the pulse repetition rates cannot be altered continuously, due to the characteristics of mode-lock laser systems, and only discrete values are possible to be selected. The substrate samples in size of $10 \times 10 \times 0.5$ mm were cut from grade 2 (ASTM B265) pure Ti sheet by a diamond saw with oil lubrication. The samples were then ground finished to 1200-grit silicate-carbon papers to remove macro-level surface defects and contaminations. Once ground, samples were ultrasonically cleaned in distilled water and dried in desiccators.

Morphology of the nanofibrous structures was characterized using Scanning Electronic Microscopy (SEM). Nanoparticle aggregation and the size of nanofibers were analyzed by Transmission Electron Microscope (TEM). Phase characteristics of the synthesized nanofibrous structures were examined using X-ray diffraction (XRD) analysis. The x-ray source was a Cu kα rotating anode generator with parallel focused beam and three-circle diffractometer with a 2-D detector. The average wavelength of the x-rays was 1.54184 Å. Phi scans with widths of 60° were implemented with the
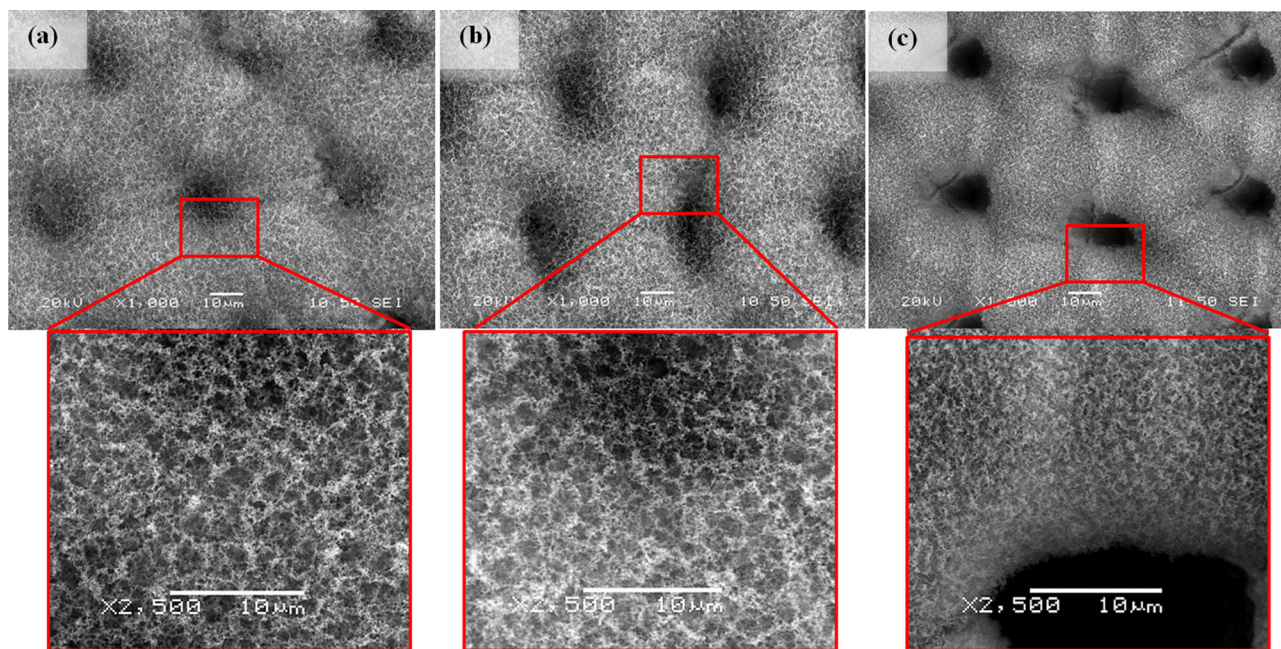
FIG. 1. SEM micrographs of titania nanofibrous structures synthesized on a Ti substrate at laser repetition of (a) 4 MHz, (b) 8 MHz, and (c) 12 MHz.

detector at four different swing angles for each sample in order to obtain a profile with a 2θ-range of 20–70°.

VI. EXPERIMENTAL RESULTS AND DISCUSSION

A. Morphology of nanostructures

The structure of the nanofibrous layer is affected by various laser parameters, such as laser fluence, laser pulse repetition, and laser pulse dwell time. In this study, we investigated the influence of laser pulse repetition on porosity, density, and size of the generated nanofibers. The ablation of Ti targets was performed at different laser pulse repetition rates from 2 MHz to 26 MHz at laser pulse dwell time of 1 ms. Figure 1 shows SEM micrographs of the nanofibrous structure synthesized on Ti substrates at pulse repetition rates of 4, 8, and 12 MHz. A close-up view of the nanofibrous layer indicates that its 3-D structure consisted of self-assembled closed rings and bridges in which nanoparticles are aggregated together. The pores in the structure are also interconnected.

The experimental results indicated that by increasing the laser pulse repletion rates from 2 MHz up to 8 MHz, the density of the generated nanostructures increases. However, increasing the repletion rate beyond 8 MHz led to a decline to the abundance of the generated nanostructures. Figure 2 presents the number of evaporated atoms predicted by Eq. (10); by increasing the laser pulse repetition rate, the number of pulses hitting the same spot for particular laser pulse dwell time increases, which leads to higher amount of ablated atoms. However, as the graph for the absorbed laser fluence in Figure 2 suggests, the increase of laser pulse repetition rates results in a reduction in laser pulse energy and consequently on the laser ablation fluence to the point that it drops below the target ablation threshold. In case of titanium target, the ablation threshold was measured to be $0.48 \, \mathrm{J/cm^2}$. Taking into account our system average laser power $P_{avg} = 10 \, \mathrm{W}$, $A_{foc} = 84.62 \times 10^{-8} \, \mathrm{cm^2}$, and titanium laser absorption coefficient for $A = 0.42$, one can see that at the pulse repetition rates higher than 8 MHz, the laser fluence merely slightly surpasses the
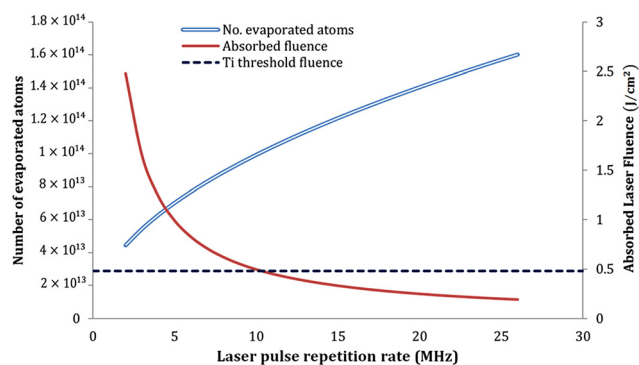

FIG. 2. The number of ablated atoms from a Ti target, ablated at different laser pulse repletion rates at laser pulse dwell time of 1 ms predicted by Eq. (10), depicted by the blue hollow line. The red solid line represents the absorbed laser fluence by the Ti target at different laser pulse repetition rates and constant average power of 10 W. The dashed line determines the laser ablation threshold of $0.48 \, \mathrm{J/cm^2}$ for Ti.
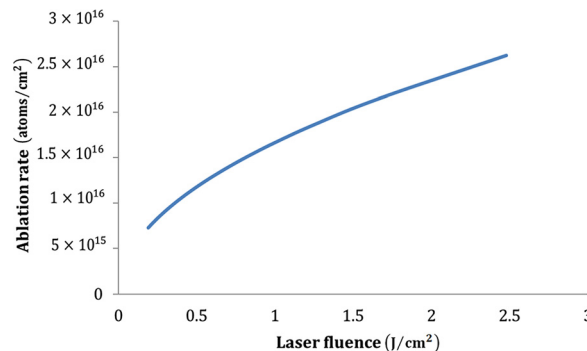

FIG. 3. The average evaporation rate for ablation by a single pulse at different laser fluences predicted by Eq. (7).
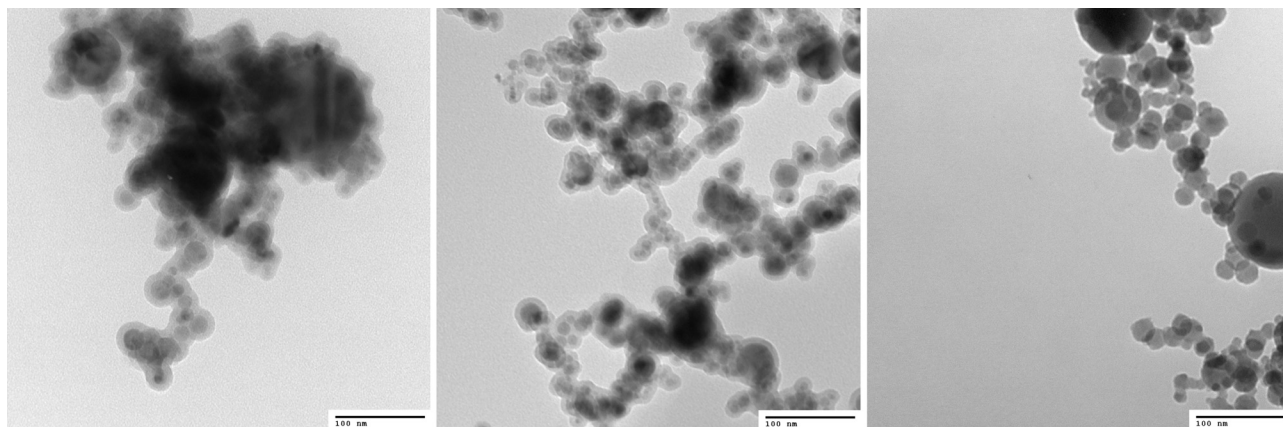
FIG. 4. TEM micrographs of Ti nanofibers synthesized at repetition (a) 4 MHZ, (b) 8 MHz, and (c) 12 MHz (the scale bar: 100 nm).

required fluence for ablating a titanium target, which may result in partial Ti ablation. This is also in good agreement with our experimental results of the ablation of Ti targets at different laser fluences.

From Eq. (10), one can predict the thermal evaporation rates in ambient air at different laser fluences. Figure 3 depicts the ablation rate at different laser fluences achieved by varying the laser pulse repetition rates at constant laser power. Assuming laser fluence of $1.2 \, J/cm^2$, Eq. (10) predicts the evaporation rate of $1.85 \times 10^{16} \, cm^{-2}$ for a Ti target. This value is in good agreement with the thermal evaporation of a Fe target in air $(1.67 \times 10^{15} \, cm^{-2})$, at laser parameters close to our experiments', reported elsewhere.[42] The higher evaporation rate for Ti may be attributed to its greater absorption coefficient $(A_{Ti} = 0.42$ and $A_{Fe} = 0.36)$ and lower thermal losses $(a_{Ti} = 0.714 \times 10^{-1} cm^2/s$ and $a_{Fe} = 2.26 \times 10^{-1} cm^2/s)$ in comparison with those for Fe, which lead to higher fluence absorption and lower heat transfer to the lattice.

To study the influence of laser pulse repetition rates on the nanofibers diameter, the synthesized nanofibers detached from the substrate and characterized by TEM. In TEM micrographs of a single nanofiber, one can observe a high degree of nanoparticle aggregation (see Figure 4). The average diameter of the nanofibers fabricated at different pulse repetition rates is depicted in Figure 5.

As mentioned before, laser fluences at laser pulse repetition rates higher than 12 MHz only slightly exceed the ablation threshold for Ti. Therefore, at repetition rate of 26 MHz

hardly any nanofibrous structures can be seen; instead, nanostructures in form of nanoparticles are generated. The empirical results indicated that a reduction in laser pulse repetition rate led to an increase in the density of the nanofibrous structures as well as in the size of nanoparticles. This can be attributed to the fact that at laser pulse repetition rates above the target ablation threshold, an accretion in repetition rates results in higher evaporation rates. The volumetric concentration of evaporated atoms in the plume strongly influences the number of primary nucleation sites.[36] Increasing the number of primary nucleation sites causes a reduction in nanofiber size. However, an increase in the laser fluence leads to the rise of plume temperature and consequently the time required for nanoparticle sticky attachment, which later results in forming larger nanofibers. As a result of finer nanofibers the pore size of the nanostructures becomes smaller, as illustrated in Figure 6.

The experimental results showed that at laser fluences above the Ti ablation threshold, an increment in laser pulse dwell time, which increases the number of laser pulses hit the same spot on the target, led to an increase in ablation rate. The deposition rate of nanostructures is analogous to the ablation rate. The results confirmed that the density of synthesized nanostructures augmented by increasing the laser pulse dwell time.

Figure 7 shows the predicted evaporation rates for the ablation of Ti targets at different laser pulse dwell times and repetitions. Laser processing of a target at laser dwell time of 1 ms and laser repetitions of 12 MHz means that 12 K pulses
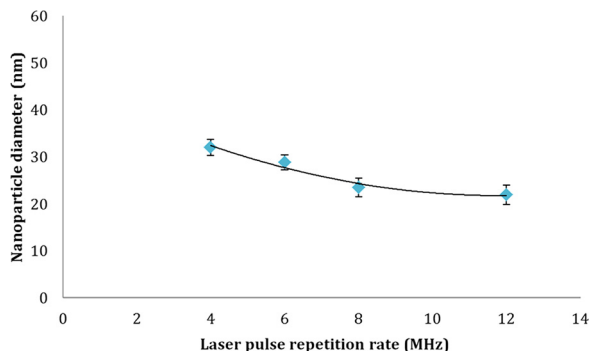

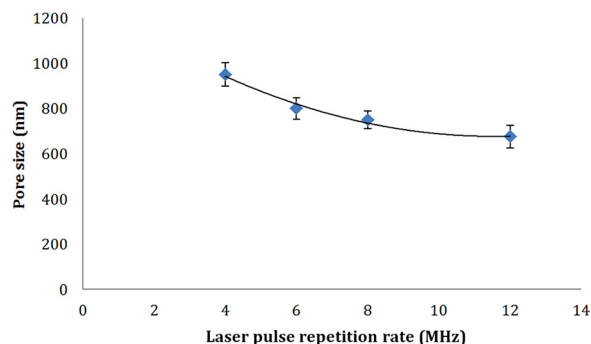FIG. 5. Measured average nanoparticle diameter at different laser pulse repletion rates.

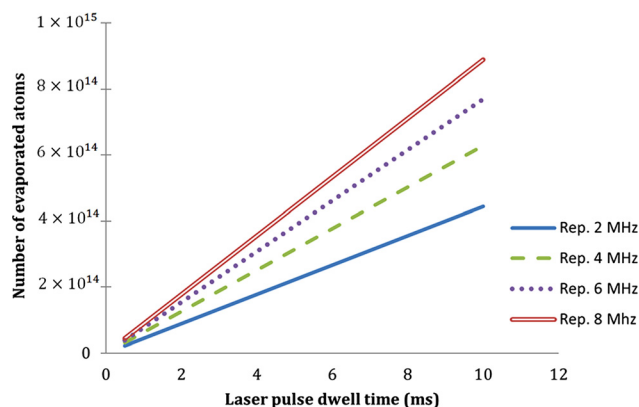FIG. 6. Measured average pore size of synthesized structures at different laser pulse repletion rates.

FIG. 7. The number of ablated atoms from a Ti target ablated at different laser dwell times and laser pulse repetition rates predicted by Eq. (10).

FIG. 8. XRD patterns of titania nanofibrous structure synthesized on Ti substrate after laser irradiation.

would arrive at the same spot on the target surface. The time interval between the pulses is 83 ns. Previous studies on the ablation of Ti in ambient air by laser intensities close to our experiment parameters suggested that plume expansion time lasts for more than 300 nm.[50,51] Therefore, one can expect the accumulation effect when laser ablating by repetition rates higher that 2 MHz.

B. Phase analysis of nanostructures

XRD analysis was performed in order to evaluate the crystal structure of the synthesized nanofibrous layer. Figure 8 shows the XRD patterns of the nanofibrous structure synthesized on Ti substrates. The unprocessed Ti substrate was entirely composed of alpha-phase titanium (α-Ti). The pattern of the nanofibrous structure, however, indicated that it consisted of tetragonal TiO_2 (rutile and anatase) and cubic TiO (hongquiite). The sharp peaks in the patterns can be attributed to the high crystallinity of the oxide phases. Titania exists in two main crystallographic forms: anatase (A) and rutile (R).[52] The XRD peaks at 2θ: 25.28° (A101) and 2θ: 27.4° (R110) are often interpreted as the characteristic
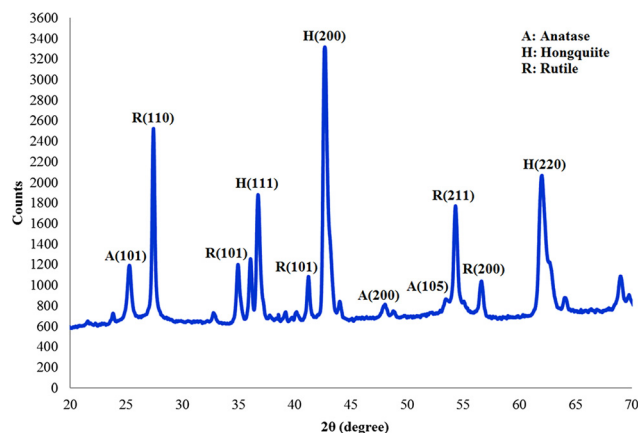
peaks of anatase and rutile crystal phases, respectively.[52,53] The peaks at 2θ: 43.37° may be associated with TiO. The mixture of anatase and rutile crystalline phases in the synthesized titania nanostructures may be connected to the changes in oxygen concentration during the ablation process. Previous studies have also suggested that there might be a definite linking between the available oxygen throughout the synthesis process and the growth of crystalline phases.[54]

Figure 9 depicts the schematic illustration of the synthesis process of titania nanostructures through the femtosecond laser ablation of Ti targets. The high temperature plume generated by laser ablation is very reactive. Thus, the presence of trace amounts of reactive gases, such as oxygen in case of ambient air, can lead to chemical reactions. The evaporated Ti atoms react with the surrounding oxygen in the front boundary of the expanding plume, and consequently, Ti-O molecular monomers are constituted. As the oxidation of Ti to generate TiO_2 is highly exothermic with the enthalpy of formation of −944.74 kJ/mol, TiO_2 molecular would be formed preferably. The generated molecules, later, collide as a result of
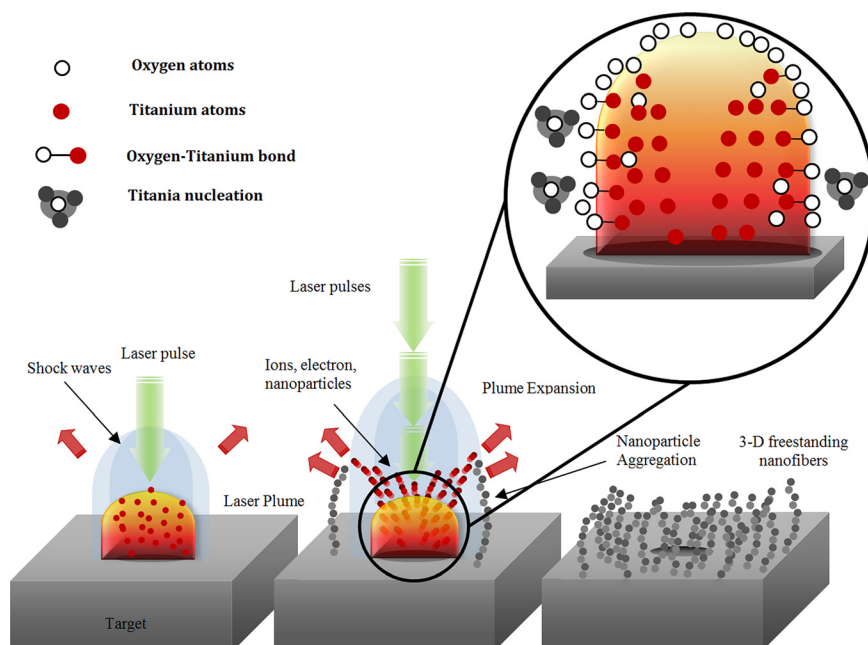

FIG. 9. Schematic illustration of the synthesis process of titania nanofibrous structure using femtosecond laser ablation of a Ti target.

thermal motion. The generated TiO_2 vapor flows to the outer wall of the plume where temperature is lower, allowing TiO_2 supersaturation which consequently results in nucleation. Once the temperature falls to the range below the boiling or sublimation point, nanostructures start to form.

VII. CONCLUSION

This study described the formation mechanism of interwoven 3-D nanofibrous structures during femtosecond laser ablation of Ti targets in ambient air. The ablation mechanism of Ti targets by successive pulses using femtosecond laser processing at background air was first demonstrated in analytical form. Later, the formation mechanism of web-like 3-D nanofibrous structures through laser ablation of Ti targets at background air was investigated. The formation of nanofibrous structures was demonstrated by applying an existing simplified kinetic model to Ti targets and ambient conditions. It was shown that the collisions between the ambient gas atoms and the target surface markedly reduced the lifetime of non-equilibrium surface state, which allowed thermal evaporation to proceed before the surface temperature dropped down. The formulas for evaporation rates and the number of ablated particles for the ablation by a single pulse and multiple pulses as a function of laser parameters, background gas, and material properties were predicted and compared to experimental results. The calculated dependence of the evaporation rate (deposition rate) on the pulse repetition rate and laser pulse dwell time was in accordance with the experimental data. The results pointed out that femtosecond laser ablation of Ti targets at air background resulted in the formation of crystalline titania nanostructures. The formation of crystalline titania nanostructures is led by thermal mechanism of nucleation and growth. The results also showed that laser pulse repetition rates could govern the density, size, and pore size of engineered nanofibrous structures. The predicted theory can be employed for predicting ablation mechanism and nanofiber formation of different materials.

ACKNOWLEDGMENTS

[1]M. Long, H. J. Rack *et al*., "Titanium alloys in total joint replacement-a materials science perspective," Biomaterials-Guildford **19**, 1621–1639 (1998).

[2]M. Jayaraman, U. Meyer, M. Bühner, U. Joos, and H. P. Wiesmann, "Influence of titanium surfaces on attachment of osteoblast-like cells in vitro," Biomaterials **25**, 625–631 (2004).

[3]R. Langer, "Biomaterials in drug delivery and tissue engineering: One laboratory's experience," Acc. Chem. Res. **33**, 94–101 (2000).

[4]W. A. McMaster, X. Wang, and R. A. Caruso, "Collagen-templated bioactive titanium dioxide porous networks for drug delivery," ACS Appl. Mater. Interfaces **4**, 4717–4725 (2012) at http://pubs.acs.org/doi/abs/10.1021/am301093k.

[5]P. Xiao, B. B. Garcia, Q. Guo, D. Liu, and G. Cao, "TiO_2 nanotube arrays fabricated by anodization in different electrolytes for biosensing," Electrochem. Commun. **9**, 2441–2447 (2007).

[6]K. Besteman, J. O. Lee, F. G. M. Wiertz, H. A. Heering, and C. Dekker, "Enzyme-coated carbon nanotubes as single-molecule biosensors," Nano Lett. **3**, 727–730 (2003).

[7]M. Paulose *et al*., "Backside illuminated dye-sensitized solar cells based on titania nanotube array electrodes," Nanotechnology **17**, 1446 (2006).

[8]G. K. Mor, K. Shankar, M. Paulose, O. K. Varghese, and C. A. Grimes, "Use of highly-ordered TiO_2 nanotube arrays in dye-sensitized solar cells," Nano Lett. **6**, 215–218 (2006).

[9]S. P. Albu, A. Ghicov, J. M. Macak, R. Hahn, and P. Schmuki, "Self-organized, free-standing TiO_2 nanotube membrane for flow-through photocatalytic applications," Nano Lett. **7**, 1286–1289 (2007).

[10]Z. Liu, D. D. Sun, P. Guo, and J. O. Leckie, "An efficient bicomponent TiO_2/SnO_2 nanofiber photocatalyst fabricated by electrospinning with a side-by-side dual spinneret method," Nano Lett. **7**, 1081–1085 (2007).

[11]C. P. Barnes, S. A. Sell, E. D. Boland, D. G. Simpson, and G. L. Bowlin, "Nanofiber technology: Designing the next generation of tissue engineering scaffolds," Adv. Drug Delivery Rev. **59**, 1413–1433 (2007).

[12]R. Jayakumar *et al*., "Fabrication of chitin–chitosan/nano TiO_2-composite scaffolds for tissue engineering applications," Int. J. Biol. Macromol. **48**, 336–344 (2011).

[13]G. Kotzar *et al*., "Evaluation of MEMS materials of construction for implantable medical devices," Biomaterials **23**, 2737–2750 (2002).

[14]G. K. Mor, O. K. Varghese, M. Paulose, and C. A. Grimes, "Transparent highly ordered TiO_2 nanotube arrays via anodization of titanium thin films," Adv. Funct. Mater. **15**, 1291–1296 (2005).

[15]G. Li Puma, A. Bono, D. Krishnaiah, and J. G. Collin, "Preparation of titanium dioxide photocatalyst loaded onto activated carbon support using chemical vapor deposition: A review paper," J. Hazard. Mater. **157**, 209–219 (2008).

[16]B. D. Yao *et al*., "Formation mechanism of TiO_2 nanotubes," Appl. Phys. Lett. **82**, 281–283 (2003).

[17]Y. Lei *et al*., "Preparation and photoluminescence of highly ordered TiO nanowire arrays," Appl. Phys. Lett. **78**, 1125 (2001).

[18]S. M. Liu, L. M. Gan, L. H. Liu, W. D. Zhang, and H. C. Zeng, "Synthesis of single-crystalline TiO_2 nanotubes," Chem. Mater. **14**, 1391–1397 (2002).

[19]X. H. Li, W. M. Liu, and H. L. Li, "Template synthesis of well-aligned titanium dioxide nanotubes," Appl. Phys. A: Mater. Sci. Process. **80**, 317–320 (2005).

[20]M. Zhang, Y. Bando, and K. Wada, "Sol-gel template preparation of TiO_2 nanotubes and nanorods," J. Mater. Sci. Lett. **20**, 167–170 (2001).

[21]J.-H. Lee, I.-C. Leu, M.-C. Hsu, Y.-W. Chung, and M.-H. Hon, "Fabrication of aligned TiO_2 one-dimensional nanostructured arrays using a one-step templating solution approach," J. Phys. Chem. B **109**, 13056–13059 (2005).

[22]J. H. Jung, H. Kobayashi, K. J. C. van Bommel, S. Shinkai, and T. Shimizu, "Creation of novel helical ribbon and double-layered nanotube TiO_2 structures using an organogel template," Chem. Mater. **14**, 1445–1447 (2002).

[23]C. L. Wong, Y. N. Tan, and A. R. Mohamed, "A review on the formation of titania nanotube photocatalysts by hydrothermal treatment," J. Environ. Manage. **92**, 1669–1680 (2011).

[24]T. Kasuga, M. Hiramatsu, A. Hoson, T. Sekino, and K. Niihara, "Formation of titanium oxide nanotube," Langmuir **14**, 3160–3163 (1998).

[25]H.-H. Ou and S.-L. Lo, "Review of titania nanotubes synthesized via the hydrothermal treatment: Fabrication, modification, and application," Sep. Purif. Technol. **58**, 179–191 (2007).

[26]A. Ghicov, H. Tsuchiya, J. M. Macak, and P. Schmuki, "Titanium oxide nanotubes prepared in phosphate electrolytes," Electrochem. Commun. **7**, 505–509 (2005).

[27]K. S. Brammer *et al*., "Improved bone-forming functionality on diameter-controlled TiO_2 nanotube surface," Acta Biomater. **5**, 3215–3223 (2009).

[28]N. Swami, Z. Cui, and L. S. Nar, "Titania nanotubes: Novel nanostructures for improved osseointegration," J. Heat Transfer **133**, 034002 (2011).

[29]Y. Bai *et al*., "The effect of annealing temperatures on surface properties, hydroxyapatite growth and cell behaviors of TiO_2 nanotubes," Surf. Interface Anal. **43**, 998–1005 (2011).

[30]O. K. Varghese, D. Gong, M. Paulose, C. A. Grimes, and E. C. Dickey, "Crystallization and high-temperature structural stability of titanium oxide nanotube arrays," J. Mater. Res. **18**, 156–165 (2003).

[31]A.-L. Papa, N. Millot, L. Saviot, R. Chassagnon, and O. Heintz, "Effect of reaction parameters on composition and morphology of titanate nanomaterials," J. Phys. Chem. C **113**, 12682–12689 (2009).

[32]Z. V. Saponjic *et al*., "Shaping nanometer-scale architecture through surface chemistry," Adv. Mater. **17**, 965–971 (2005).

[33]K. Vasilev *et al*., "Tailoring the surface functionalities of titania nanotube arrays," Biomaterials **31**, 532–540 (2010).

[34]N. F. Fahim and T. Sekino, "A novel method for synthesis of titania nano-tube powders using rapid breakdown anodization," Chem. Mater. **21**, 1967–1979 (2009).

[35]J. Perrière, C. Boulmer-Leborgne, R. Benzerga, and S. Tricot, "Nanoparticle formation by femtosecond laser ablation," J. Phys. D: Appl. Phys. **40**, 7069–7076 (2007).

[36]M. Ullmann, S. K. Friedlander, and A. Schmidt-Ott, "Nanoparticle formation by laser ablation," J. Nanopart. Res. **4**, 499–509 (2002).

[37]X. B. Chen, Y. C. Li, P. D. Hodgson, and C. Wen, "The importance of particle size in porous titanium and nonporous counterparts for surface energy and its impact on apatite formation," Acta Biomater. **5**, 2290–2302 (2009).

[38]A. Tavangar, B. Tan, and K. Venkatakrishnan, "Synthesis of bio-functionalized three-dimensional titania nanofibrous structures using femtosecond laser ablation," Acta Biomater. **7**, 2726–2732 (2011).

[39]B. Tan and K. Venkatakrishnan, "Synthesis of fibrous nanoparticle aggregates by femtosecond laser ablation in air," Opt. Express **17**, 1064–1069 (2009).

[40]E. G. Gamaly, A. V. Rode, B. Luther-Davies, and V. T. Tikhonchuk, "Ablation of solids by femtosecond lasers: Ablation mechanism and ablation thresholds for metals and dielectrics," Phys. Plasmas **9**, 949 (2002).

[41]E. G. Gamaly, A. V. Rode, and B. Luther-Davies, "Ultrafast ablation with high-pulse-rate lasers. Part I: Theoretical considerations," J. Appl. Phys. **85**, 4213 (1999).

[42]E. G. Gamaly et al., "Ablation of metals with picosecond laser pulses: Evidence of long-lived non-equilibrium surface states," Laser Part. Beams-Pulse Power and High Energy Densities **23**, 167–176 (2005).

[43]I. A. Zel'dovich, Physics of Shock Waves and High-Temperature Hydrodynamic Phenomena (Dover, 2002).

[44]E. G. Gamaly, "The physics of ultra-short laser interaction with solids at non-relativistic intensities," Phys. Rep. **508**, 91–243 (2011).

[45]B. Tan, A. Dalili, and K. Venkatakrishnan, "High repetition rate femtosecond laser nano-machining of thin films," Appl. Phys. A **95**, 537–545 (2008).

[46]K. Venkatakrishnan, B. Tan, P. Stanley, L. E. N. Lim, and B. K. A. Ngoi, "Femtosecond pulsed laser direct writing system," Opt. Eng. **41**, 1441 (2002).

[47]M. D. Perry et al., "Ultrashort-pulse laser machining of dielectric materials," J. Appl. Phys. **85**, 6803–6810 (1999).

[48]B. Luther-Davies, A. V. Rode, N. R. Madsen, and E. G. Gamaly, "Picosecond high-repetition-rate pulsed laser ablation of dielectrics: The effect of energy accumulation between pulses," Opt. Eng. **44**, 051102 (2005).

[49]E. G. Gamaly,, N. R. Madsen, D. Golberg, and A. V. Rode, "Expansion-limited aggregation of nanoclusters in a single-pulse laser-produced plume," Phys. Rev. B **80**, 184113 (2009).

[50]M. Cirisan, J. M. Jouvard, L. Lavisse, L. Hallo, and R. Oltra, "Laser plasma plume structure and dynamics in the ambient air: The early stage of expansion," J. Appl. Phys. **109**, 103301 (2011).

[51]A. De Giacomo, M. Dell'Aglio, A. Santagata, and R. Teghil, "Early stage emission spectroscopy study of metallic titanium plasma induced in air by femtosecond-and nanosecond-laser pulses," Spectrochim. Acta, Part B **60**, 935–947 (2005).

[52]L. Jing et al., "Effects of surface oxygen vacancies on photophysical and photochemical processes of Zn-doped TiO_2 nanoparticles and their relationships," J. Phys. Chem. B **110**, 17860–17865 (2006).

[53]Q. Zhang, L. Gao, and J. Guo, "Effects of calcination on the photocatalytic properties of nanosized TiO_2 powders prepared by $TiCl_4$ hydrolysis," Appl. Catal. B **26**, 207–215 (2000).

[54]I. Banerjee et al., "Effect of ambient pressure on the crystalline phase of nano TiO_2 particles synthesized by a dc thermal plasma reactor," J. Nanopart. Res. **12**, 581–590 (2010).